**PROBING THE LUNAR SURFACE USING SPATIALLY RESOLVED OPTICAL AND NEAR-IR IMAGING POLARIMETRY WITH *HST*/ACS AND *HST*/NICMOS.**
Dean C. Hines[1], Yuriy Shkuratov[2], Misha Kreslavsky[3], Glenn Schneider[4], Gorden Videen[1], Michael Sitko[1], Heidi B. Hammel[1] and Michael J. Wolff[1] ([1]Space Science Institute, 4750 Walnut Street, Suite 205, Boulder, CO 80301, [2]Astronomical Institute of Kharkov National University, 35 Sumskaya St., Kharkov, 61022, Ukraine, [3]Geological Sciences, Brown University, Box 1846, Providence, RI 02912-1846, [4]The University of Arizona, 933 N. Cherry Ave., Tucson, AZ 85721).

**Introduction:** Interest in the Moon as both a destination for human spaceflight and a platform for astronomical observatories has placed a new emphasis on understanding details of the lunar regolith. In particular, NASA's Strategic Plan, Goal 6 expresses the need for studies to determine requirements for future missions, and "robotic missions will survey and characterize potential lunar landing sites… and take measurements to characterize the Moon's surface and the space environment in support of science objectives." In addition, NASA's Science Mission Directorate 2007-2016 contains text from the *The Scientific Context for the Exploration of the Moon* (NRC, 2006) encouraging studies to: "Constrain processes involved in regolith evolution and decipher ancient environments from regolith samples."

Here we briefly discuss *HST*/ACS (optical) and *HST*/NICMOS (near-IR) polarimetric observations of the Moon that will place direct constraints on regolith grain size and "roughness." Such constraints will locate regions of fresh *vs.* mature (processed) material that could affect the selection of sights for future investigation and exploration, and elucidate the evolution of dusty material on the Moon.

**Lunar Regolith:** The nature and evolution of lunar regolith is both practically and fundamentally interesting. Measurements of the grain-size distributions will aid in the evaluation of dusty lunar environments both for human sorties and potential sites for lunar facilities. Composition and grain size distribution, and the effects of space weathering are also crucial for understanding the structure and evolution of the Moon.

Exposure to charged particles and micrometeor bombardment causes accumulation of nanophase reduced iron ($npFe^0$) on lunar regolith grains, decrease in grain size, and enrichment with glass material and agglutinates. Examples of immature regolith include disturbed areas such as young impact craters and "swirls," which are structures postulated to arise from cometary or meteoroid swarm encounters [e.g., 1-3]. The evolution from immature to mature grains is manifested in their spectral and polarimetric properties.

**Imaging Polarimetry of the Lunar Surface:** Sunlight scattered by the lunar regolith is linearly polarized (Fig. 1).
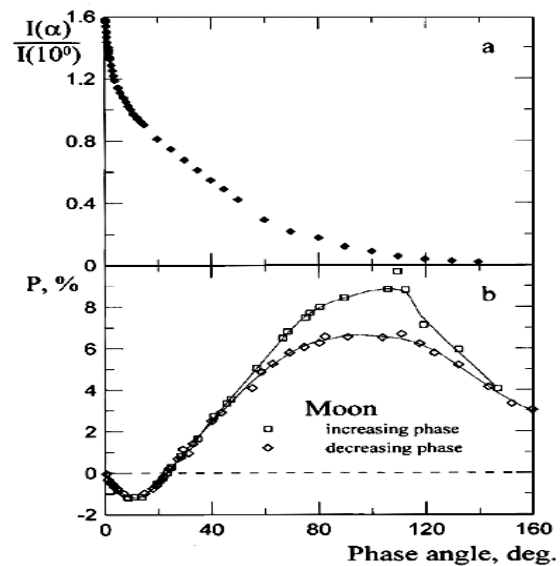


**Fig. 1.** Scattered light from the Moon. Total intensity (top) and linear polarization (bottom) as a function of phase angle ($\alpha$). The (+) and (-) signify that the plane of polarization is normal and parallel to the plane of scattering, respectively. [after 4]

The degree of polarization is a function of wavelength, the scattering phase angle ($\alpha$: Fig. 1), the roughness of the surface, and the mean grain size ($d$). For large phase angles, the wavelength–dependent degree of polarization ($P$) is correlated with the albedo ($A$). This "Umov's Law" is approximately linear on a log–log scale: $\log P + a \log A = b$, where $a$ and $b$ are constants [e.g., 5], and $a$ can approach 0.95. However, deviations from this simple correlation, quantified by the parameter $(P_{max})^\alpha A$, have been demonstrated to provide significant information on the characteristic grain size and microporosity of the lunar regolith [e.g., 6,7,8]. Laboratory measurements of lunar samples

and lunar regolith simulants have shown that the variations of this parameter are closely correlated with the particle size [6, and references therein]. Figure 2 shows how the parameter $(P_{max})^{\alpha}A$ distinguishes grain-size populations; young craters are more clearly visible in Fig. 2c indicating their coarse regolith particles.
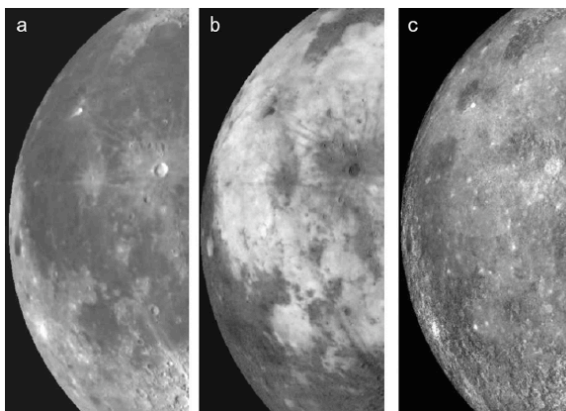


**Fig. 2.** Earth-based telescope photopolarimetric images of the western part of the lunar nearside at phase angle 88°: (a) an albedo image after compensation of the brightness trend from limb to terminator, (b) an image of polarization degree, and (c) an image of deviation from Umov's law. i.e., the parameter $(P_{max})^{\alpha}A$. [after 9]

**Measuring Grain Sizes via Polarimetry:** The median scattering grain size can be constrained by polarization measurements as a function of phase angle [e.g., 7]. Figure 3 shows how grain size affects the polarization as a function of phase angle.
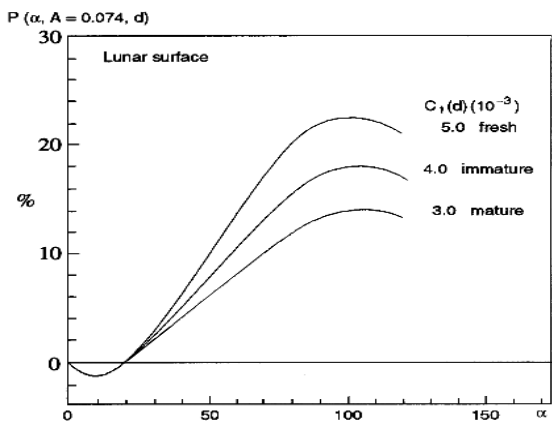


**Fig. 3.** Phase angle dependence of Umov's Law, expressed by polarization $P$, for albedo $A = 0.074$. Three values of the grain size parameter $C1(d)$ from [6] correspond to fresh, immature, and mature lunar surfaces. [after 7]

Using high spatial resolution, the $(P_{max})^{\alpha}A$ and grain-size parameters can be exploited to provide a detailed quantitative map of regolith grain size by fitting a polarization data cube that has two spatial dimensions and one phase dimension.

**Multi-band Imaging Polarimetry:** Spatially resolved polarimetry over large wavelength ranges further characterizes the regolith. Since polarization fractions are both grain-size *and* wavelength dependent (for any phase angle), ratios of polarization fractions at *multiple* wavelengths provide very strong constraints in determining grain sizes. Figure 4 illustrates this with $C_{\perp}$ (plus polarization) and $C_{\parallel}$ (minus polarization) constructed from just a single ratio (0.65/0.42 μm). Using optical (provided by ACS) and near-IR (provided by NICMOS) polarimetric imaging together will provide multiple ratios over a large range of wavelengths (~ 0.3 to 2.0 μm), providing a powerful diagnostic to characterize the lunar regolith.
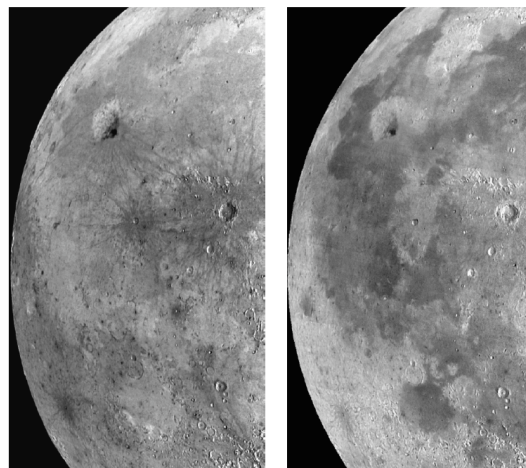


**Fig. 4.** Example images of $C_{\parallel}$(0.65/0.42 μm) and $C_{\perp}$(0.65/0.42 μm), which are sensitive to somewhat different thicknesses of the surfaces of regolith grains. [after 9]

**The Need for *HST*:** Despite the power of polarimetry, none of the current or planned lunar orbiter missions, including the Lunar Reconnaissance Orbiter (LRO: USA), Chandrayaan-1 (India), Chang'e 1 (China), or Kaguya (Japan), are equipped with polarimetric optics. The spatial resolution of these missions will be ~ 20–200 m. From Earth, these size-scales bracket the spatial resolutions of ACS and NICMOS. Current ground-based instrumentation can achieve comparable resolutions in the near IR with adaptive optics over limited FOVs, but such techniques are

untested and unproven for lunar observations due to the combination of the Moon's large spatial extent, brightness, and non-sidereal rate. Such resolution is not available to ground-based telescopes in the visible. Therefore, *HST* is the only platform providing *contemporaneous* imaging polarimetry over the entire optical and near-IR wavelength range at spatial scales comparable with lunar reconnaissance missions, and with a stable FOV.

When the resolution of spectro- and photometric imaging increased from that of ground-based capabilities to that of Clementine (~100 m), our ability to detect the spectral inhomogeneity of the surface increased dramatically and produced many interesting results [e.g., 10,11]. We anticipate that polarimetry at the spatial resolutions afforded by *HST* (comparable to that of orbital missions) will likewise bring interesting and unexpected results, and may show the critical need for orbiting polarimeters on future missions.

**Feasibility:** Careful calibration and data analysis of ACS polarimetric data can produce absolute accuracy in the degree of polarization better than 0.5% and detection of features with polarization degree contrast as small as 0.2% (Fig. 5: after [12]). The instrumental polarization of NICMOS is <1% [13], so we expect similar or superior performance [14] for lunar observations.
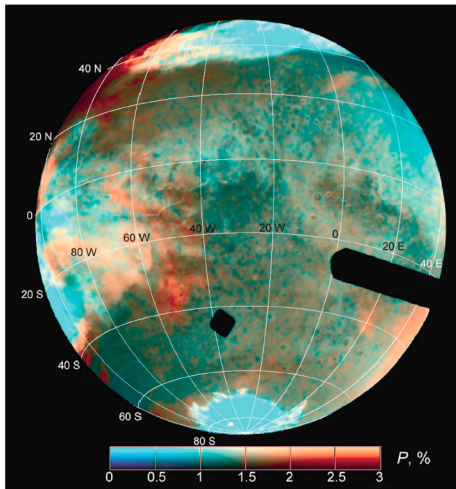


**Fig. 5.** ACS imaging polarimetry of Mars. [after 12]

Observations with the ACS polarizers combined with wide or narrow filters would require about 0.2 and 2s, respectively, which is short enough to minimize smearing of the FOV while on gyros. However, 2μm polarimetry with NICMOS camera 2 (NIC2) requires Bright Object (BO)

mode. On-orbit, this mode is used in support of BO coronagraphy, but calibration linearity data in BO mode is not taken as part of STScI's normal calibration program. The calibratability (linearity correction) for BO mode (specifically for the required per-pixel exposure times of 10, 20, 40, and 80 ms) was demonstrated by the NICMOS Instrument Definition Team, during System Level Thermal Vacuum tests. Thus, an on-orbit NIC2 BO polarimetry calibration campaign would be required as an adjunct to the science observations.

**Targets:** Prime areas for investigation at optimum phase angles (~80-110˚) using *HST* include the Apollo 17, Luna 16 and 24 landing sites, Marius Hills, Plateau Aristarchus, the Reiner-γ formation and Rümker dome. In addition, the LCROSS piggyback mission aboard LRO is planned to impact the Moon in 2009, and will produce a freshly disturbed site that is could be ideal for *HST* imaging polarimetry. NICMOS camera 2 contains narrow band filters that span the 2 μm water absorption band, so a combined narrow band and imaging polarimetry campaign could provide important contemporaneous support observations for the LCROSS experiment.

**Conclusions:** The two polarimetric imaging systems aboard *HST* (ACS & NICMOS) can provide high fidelity optical and near-IR imaging polarimetry with sub-km resolution comparable to that obtained by lunar reconnaissance missions that only have direct imaging. These complementary *HST* observations will yield strong constraints on the grain size and texture of the regolith.

**References:** [1] Schultz P. & Srnka L. (1980), *Nature* 284, 22-26. [2] Pinet, P. et al. (2000) *JGR*, 105, 9457. [3] Starukhina L. & Shkuratov Yu. 2004, *Icarus* 167, 136. [4] Shkuratov et al. 2004, in *Photopolarimtry in Remote Sensing*, NATO Science Series, 161, 191. [5] Dollfus, A. & Bowell, E. 1971, *A&A*, 10, 29. [6] Shkuratov, Yu. & Opanasenko, N.V. 1992, *Icarus*, 99, 468. [7] Dollfus, A. 1998, *Icarus*, 136, 69. [8] Dollfus, A. 1999, *Icarus*, 140, 313. [9] Shkuratov, Y. et al. 2007, *Icarus*, 187, 406. [10] Pieters et al. 1994, *Science*, 266, 1844. [11] Kreslavsky & Shkuratov, 2003, *J. Joephys.res*. 108, DOI 10.1029/2002JE001937. [12] Shkuratov, Y. et al. 2005, *Icarus*, 176, 1. [13] Hines, D.C. et al. 2000, *PASP*, 112, 983. [14] Batcheldor, D. et al. 2006, *PASP*, 118, 642.